Reliability Engineering and System Safety 257 (2025) 110866

Contents lists available at ScienceDirect

Reliability Engineering and System Safety

journal homepage: www.elsevier.com/locate/ress

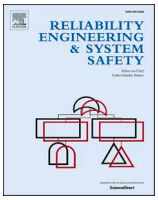

A systematic resilience assessment framework for multi-state systems based on physics-informed neural network

Yuxuan He [a], Enrico Zio [b,c], Zhaoming Yang [a], Qi Xiang [d,a], Lin Fan [e], Qian He [a], Shiliang Peng [a], Zongjie Zhang [f], Huai Su [a,*], Jinjun Zhang [a,*]

[a] National Engineering Laboratory for Pipeline Safety/ MOE Key Laboratory of Petroleum Engineering /Beijing Key Laboratory of Urban Oil and Gas Distribution Technology, China University of Petroleum-Beijing, 102249, Beijing, China
[b] Dipartimento di Energia, Politecnico di Milano, Via La Masa 34, 20156, Milano, Italy
[c] Centre de recherche sur les Risques et les Crises (CRC), Mines Paris, PSL University, Sophia Antipolis, France
[d] CNOOC Research Institute Ltd., Beijing 100028, China
[e] PetroChina planning and engineering institution, China
[f] PipeChina Hunan Pipeline Co., Ltd, Hunan, China

ARTICLE INFO

Keywords:
Resilience
Multi-State System
Markov Repairable Process
Physics-informed Machine Learning

ABSTRACT

Resilience is crucial for systems to maintain functionality under disturbances, especially in critical applications. However, current methods for assessing resilience in multi-state systems (MSS), particularly those modeled with Markov Repairable Processes (MRP), often face high computational costs and inefficiencies in handling complex dynamics. To address these issues, this paper proposes a systematic framework for resilience assessment of MSS whose recovery process is described as a MRP, integrated with enhanced Physics-Informed Neural Networks (PINN). In the first step of the framework, the computation of resilience indices is performed, based on the MRP of the MSS and considering the system evolution through vulnerable and recovery phases. In the second step of the framework, the enhanced PINN is integrated into the MRP solution. A typical standby MSS structure is analyzed based on the proposed framework. By gradient calibration and momentum-driving training, the computational cost is shown to be reduced by 92.4 %, compared to the eigenvector method of solution. The approach is adaptable to other safety-critical systems, offering a robust tool for more effective resilience evaluation and system optimization.

1. Introduction

Integrity and reliability analyses have proven effective in facilitating safety assessments of systems. Integrity primarily considers the intrinsic structure of the system under evaluation but often lacks a comprehensive systematic analysis [1]. Reliability looks at the achievement of predefined functions under normal operation [2,3]. However, reliability does not consider recovery after the system has suffered a major disturbance. As the complicating of the system structure and functions, some units in the system become the core of the system inevitably. For example, units such as the compressors in natural gas supply [4], or the hydrogen production apparatus in hydrogen energy supply [5]. These units may become non-operational when the system encounters sizable natural disasters. Then, the system tends to breakdown. For critical systems and infrastructures, it is crucial to evaluate the recovery capability of the system after a severe disturbance [6,7].

To this aim, the concept of resilience of a system has been introduced to measure the system's ability to resist, absorb, and promptly recover from external disturbances. Resilience has been used for assessing natural disaster adaptation for power grids [8,9] and nuclear power plants [10]. For the resilience assessment and optimization of engineering systems, a suitable approach is to model them systems as Multi-State Systems (MSS) [11]. The evolution of MSS is described as a stochastic process of transition across a finite number of intermediate states representing of performance levels between normal operation and breakdown. The rich intermediate states in MSS models enable a more granular representation of the degradation behavior of engineering systems.

Markov Repairable Process (MRP) can be used for the time-evolving probabilistic representation of the states transition process in the MSS [12]. A system of ordinary differential equations (ODE) is used to

* Corresponding author
E-mail addresses: suhuai@cup.edu.cn (H. Su), zhangjj@cup.edu.cn (J. Zhang).

https://doi.org/10.1016/j.ress.2025.110866
Received 19 March 2024; Received in revised form 19 September 2024; Accepted 27 January 2025
Available online 30 January 2025
0951-8320/© 2025 Elsevier Ltd. All rights are reserved, including those for text and data mining, AI training, and similar technologies.

Nomenclature

ADAM	adaptive moment estimation
$C(t)$	maintenance cost for the system
DNN	deep neural network
FNN	feed-forward neural network
$L(\boldsymbol{\theta})$	total loss of the physics-informed neural network
MRP	markov repairable process
MSS	multi-state system
MCS	monte-carlo simulation
NADAM	nesterov-accelerated adaptive moment estimation
NAG	nesterov accelerated gradient
ODE	ordinary differential equations
p	probability of unsuccessful switching
PINN	physics-informed neural network
$\mathbf{P}(t)$	state transition probability matrix
$\mathbf{P}'(t)$	state transition matrix
$\mathbf{Q}(t)$	state transition rate matrix
$\mathbf{Q}_{\mathrm{I}}$	state transition rate matrix for system I
$\mathbf{Q}_{\mathrm{II}}$	state transition rate matrix for system II
$\mathbf{Q}_{\mathrm{III}}$	state transition rate matrix for system III
$\mathbf{Q}_{\mathrm{IV}}$	state transition rate matrix for system IV
RK	runge-kutta
RMSE	root mean square error
RMSProp	root mean square error propagation
$\mathbf{S}$	system state space
$\mathbf{S}_0$	state vector for the system in healthy condition
S_f	failure state
$\mathbf{S}_i$	state vector for the system in vulnerable states i
S_b	standby state
$\mathbf{S}_n$	state vector for the system in breakdown state
S_w	normal operational state
α	conversion factor for the repair rate
ε	slack variable in network training
$\lambda(t)$	failure rate of the system
λ_A	failure rate of unit A in working state
λ_B	failure rate of unit B in working state
λ_B^s	failure rate of unit B in standby state
$\mu(t)$	repair rate of the system
μ_A	repair rate of unit A
μ_B	repair rate of unit B
μ_t	repair rate when the system is in breakdown state
μ_g	converted repair rate
$\boldsymbol{\varphi}_{\mathrm{t}}$	resilience indices set
$\varphi_{\mathrm{resist}}$	resistance of the system in vulnerable phase
φ_{a}	absorptivity of the system in vulnerable phase
φ_{v}	vulnerability of the system in vulnerable phase
$\varphi_{\mathrm{recover}}$	recoverability for the system in recovery phase
$\widehat{\boldsymbol{\Phi}}(t;\boldsymbol{\theta})$	output vector of the neural network
Δ_0	gradient j the initial state
Δ_i	gradient for the ith transition equation
Δ_s	origin gradient for the transition equation
Δ'_s	calibrated gradient for the transition equation

represent mathematically the system transition process. But its solution may present significant challenges. Firstly, expanding the state space complicates the solution, particularly for non-homogeneous MRP or semi-MRP. Secondly, the computational cost increases with the time granularity. As a consequence, when solving high-dimensional MRP matrices, numerical solution methods such as Runge-Kutta (RK) [13] and Monte-Carlo simulation (MCS) [14,15] are computationally demanding, especially when dealing with safety-critical applications requiring uncertainty and sensitivity analyses with batch computing.

Given the limitations of these traditional methods, there is a pressing need for more efficient and scalable approaches to solving MRPs [16], particularly in the context of resilience assessment. Physics-Informed Neural Networks (PINNs) have recently emerged as a promising alternative, integrating physical laws directly into the neural network's architecture to offer more efficient solutions without requiring extensive datasets. However, the application of PINNs to MRPs introduces its own challenges, notably the potential for gradient conflicts during training, which can hinder convergence and accuracy.

This study aims to enhance the stability and accuracy of PINNs for solving MRPs by introducing a novel gradient calibration method. This method seeks to address the gradient conflict issues inherent in multi-task training within PINNs, thereby improving their effectiveness in resilience assessment for MSS.

By overcoming these challenges, the proposed approach has the potential to significantly improve the computational efficiency and accuracy of resilience assessments in complex systems. This, in turn, can lead to better-informed decisions in the design and management of critical infrastructures, ensuring they are more resilient to disruptions and capable of rapid recovery.

2. Literature review and original contributions

2.1. Resilience definition for MSS and indices

Resilience, derived from the Latin word resiliere meaning "to bounce back," is a concept applied across diverse fields such as critical infrastructure, ecology, and engineering. Initially introduced by Holling [17] in ecological studies, resilience has expanded to include a system's ability not only to recover from disruptions but also to resist and absorb potential damages. This broader perspective is especially vital in critical infrastructure, where maintaining functionality during and after disruptions is essential.

Resilience studies often describe systems as undergoing three key stages when faced with disruptive events: resistance, absorption, and recovery [18–20].

- **Resist stage**: The key in the resist stage is the ability to resist to external disturbances to the system.
- **Vulnerable stage**: The vulnerable stage refers to the system's ability to absorb external disturbances and reserve a certain working capability after being disturbed.
- **Recovery stage**: The recovery stage investigates the system's recovery ability after the external disturbances.

Based on these stages, various resilience indices have been developed to assess a system's resilience comprehensively [21]. Table 1 summarizes the indices used in previous studies, categorizing them according to the Resist, Vulnerable, Recovery stages and the global perspective of the system resilience. Despite differences in terminology and definitions, these indices consistently capture the core aspects of system resilience, underscoring their effectiveness in evaluating and modeling resilience in complex systems.

In modeling MSS using the MRP, the transition between transient and steady states is crucial for analyzing system resilience. Traditional methods have approached the quantification of resilience across the three stages in various ways. Building on these models and inspired by [32], our approach focuses on integrating the transition from transient to steady states into resilience indices using an integral method. This allows for a more comprehensive quantification of the system's overall resilience.

Table 1
Perspective of resilience assessment and related indices

Reference	Year	Indices			
		Resist stage	Vulnerable stage	Recovery stage	Global perspective for three stages
Bruneau [19]	2003	Robustness	Absorbability	Rapidity	-
Rose [22]	2007	Robustness	Absorbability	Rapidity	-
Zobel [23]	2011	Robustness	Absorbability	Rapidity	Overall resilience
Francis [24]	2014	Robustness	Absorbability	Recoverability	-
Zobel [25]	2014	-	-	-	Predicted resilience and partial resilience
Zhang [26]	2018	-	-	-	System resilience
Zeng [27]	2021	Resistance	Absorbability	Recoverability	-
Zeng [28]	2021	Resistance	Absorbability	Recoverability	Overall resilience
Yang [29]	2023	Resistance	Vulnerability	Recoverability	-
Tan [30]	2023	Resistance	Absorbability	Recoverability	Inherent and acquired overall resilience
Dui [31]	2024	Resistance	Absorbability	Recoverability	Overall resilience
Our Work	**2024**	**Resistance**	**Absorptivity, Vulnerability**	**Recoverability**	**The cumulative of the system's evolution has been considered**

- denotes not being considered.

The perspectives considered at each stage in our paper are as follows:

- **Resistance** during the resist stage.
- **Absorptivity** and **vulnerability** during the vulnerable stage.
- **Recoverability** during the recovery stage.

These indices, derived from a thorough review of existing research, address the limitations of traditional models by incorporating the transient aspects of the MRP. This approach is particularly applicable to complex systems with multi-state transitions, ensuring that resilience assessments are both robust and relevant to real-world scenarios.

2.2. MRP solution and PINN

In the realm of MSS, the MRP is frequently employed to model the probabilistic state transitions over time, capturing the stochastic behavior of such systems [33–35]. Traditional numerical methods, such as Runge-Kutta (RK) and Monte Carlo Simulations (MCS), have been extensively utilized to solve MRPs. For instance, RK methods have been successfully applied to solve ordinary differential equations (ODEs) associated with MRPs, providing accurate solutions for system reliability analysis [13]. Similarly, MCS is widely adopted for probabilistic assessments of Markov chains, particularly in the context of complex systems with expansive state spaces, where it provides robust estimates of system state distributions over time [14,15].

Despite their widespread use, these traditional methods present notable limitations. As the state space of the system expands or the system exhibits non-homogeneous behavior, the computational cost of applying RK and MCS becomes increasingly prohibitive [36]. This challenge is especially pronounced in safety-critical applications, where high computational efficiency is required to perform uncertainty and sensitivity analyses in a timely manner [37].

Given these challenges, there is a clear need for more efficient and scalable solutions for MRP problems. This is where PINNs come into play [36,38–40]. PINNs offer a novel approach by embedding the physical laws governing the MRP directly into the neural network structure. Unlike traditional neural networks that require large amounts of data for training [41], PINNs leverage the governing differential equations and initial conditions of the MRP, enabling them to solve these problems with higher efficiency and without the need for extensive datasets.

The construction of a PINN for MRP begins with the establishment of a Deep Neural Network (DNN) as a surrogate model for the ODE-based MRP solution. A Feed-Forward Neural Network (FNN) is often employed in this context due to its simplicity and effectiveness in solving ODEs. The training of the FNN involves two main processes: forward propagation and backpropagation. During forward propagation, time variables are used as inputs, and the network produces an output that approximates the solution of the MRP. The network parameters are iteratively adjusted during backpropagation to minimize the loss function, which measures the discrepancy between the network output and the physical laws governing the MRP.

A critical aspect of the PINN approach is the calculation of the residuals, which quantify how well the network output satisfies the MRP's governing equations. These residuals are computed using the Automatic Differentiation (AD) [42] algorithm, which precisely calculates derivatives for functions expressed as computational graphs, such as those found in neural networks. This eliminates the need for approximation methods, such as finite difference schemes, and reduces errors associated with truncation and rounding. Furthermore, PINNs are mesh-free methods, meaning they do not require a discretized mesh to solve the ODEs, which simplifies the solution process.

However, one challenge with PINNs is the potential for conflicting gradients during the training process, particularly when dealing with multiple loss functions derived from different physical laws [43]. This conflict can result in non-convergence or slow convergence of the neural network. To mitigate this issue, a gradient calibration method has been proposed. This method adjusts the conflicting gradients to ensure that the network training is balanced and that useful information from all gradients is utilized. By resolving these conflicts, the trained PINN can provide more accurate results and achieve faster convergence.

In summary, while traditional methods for solving, MRPs are computationally intensive and may not scale well with complexity, PINNs offer a promising alternative by integrating physical laws into the neural network framework. However, to fully leverage the potential of PINNs, it is crucial to address the challenges associated with gradient conflicts during training. The gradient calibration method proposed in this paper provides a feasible solution to this problem, offering a more reliable and efficient approach to MRP-based resilience assessment in MSS.

2.3. Original contribution

This work aims to address the challenges of non-homogeneous resilience in MSS by proposing a systematic method for resilience assessment using a PINN-based solution for MRP. The key contributions are as follows:

(1) Novel resilience indices are proposed taking into account the non-homogeneous nature of MSS. These indices—resistance, absorptivity, vulnerability, and recoverability—enable a dynamic and cumulative evaluation of the system.
(2) A PINN-based solver has been introduced, enhancing computational efficiency and providing stable, accurate solutions for high-dimensional MRPs. Gradient calibration with NADAM accelerates convergence and reduces computational costs by up to 92.4 %, giving contribution to rapid and scalable resilience assessments.

(3) The framework has been applied to classical standby MSS structures, effectively capturing system resilience dynamics. It supports resilience evaluation for a wide range of standby systems and is adaptable to other complex engineering systems.

2.4. Paper organization

The remainder of this paper is organized as follows: Section 2 elaborates on the details of the proposed resilience evaluation method, including the resilience indices modeling for MSS and the solution of MRP based on PINN. Section 3 tests the proposed modeling method by applying it for the calculations of four classical standby systems. Finally, Section 4 concludes the paper.

3. Methodology

The proposed resilience assessment methodology is presented in detail in this section (Fig. 1). It is outlined in two main parts: resilience modeling and solution. In the first step, the resilience interval is defined, encompassing the system's evolution from disturbance to recovery, and

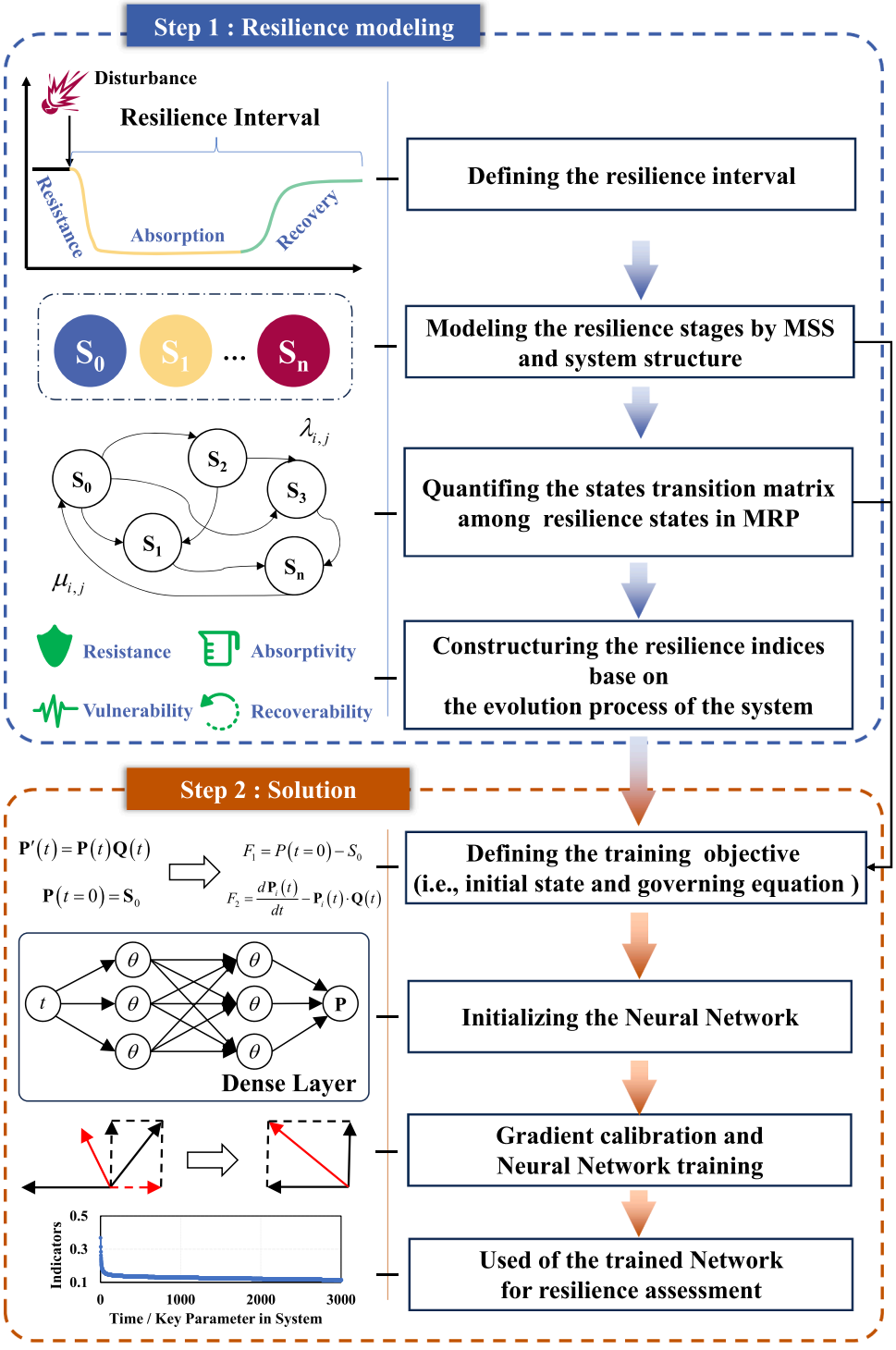

Fig. 1. Proposed methodology of resilience assessment

MSS and MRP are employed to model and assess resilience during this period. In the second step, the key solution processes are addressed by introducing a gradient-corrected PINN, leading to the determination of the system's resilience indices.

3.1. Theoretical framework for resilience formulation

This subsection provides a systematic introduction to the modeling process within the proposed resilience assessment methodology. The modeling consists of two main steps. In the first step, the process of the MSS being disturbed and recovered is modeled as MRP. In the second step, resilience indices are proposed for evaluation.

3.1.1. MSS resilience modelling

The core of system resilience modeling focuses on the process from disturbance to recovery. As shown in Fig. 2, this paper divides the system's resilience into two phases: the vulnerable phase, from disturbance to the start of remedial actions, and the recovery phase, where the system's function is restored, returning to an imperfect operational state.

Assume a system starts in a normal operational state. When the system encounters disturbances of varying magnitudes, its performance—such as the probability of remaining in a normal operational state $\mathbf{P}(X(t) = \mathbf{S_0})$—declines, entering the vulnerable phase. At the moment of disturbance, performance drops rapidly. Assuming the system has some self-repair capability, this decline will gradually slow down. However, it might still breach the acceptable performance threshold, leading to a potential breakdown state. At this point, timely repairs are needed to push the system into the recovery phase, ensuring its function and guiding it back toward a normal operational state.

Consider a system exposed to three levels of disturbance: If the disturbance is too severe, remedial measures may be ineffective, resulting in system breakdown. If the disturbance is acceptable and repairs are timely, the system can recover to its normal operational state through a combination of self-repair and external remedies. However, untimely repairs might still result in failure.

Further, MSS is introduced to describe the resilience states of the system. Consider the performance of a MSS is characterized by $n+1$ discrete ordered states represented by the following collection:

$$\mathbf{S} = \{0, 1, \ldots, n\} \tag{1}$$

where 0 denotes the initial state, and n denotes the final state in the system evolution. The others are the intermediate states. Considering the transformation of the system between different states, the conversion rate matrix is introduced as $\mathbf{Q}(t)$.

$$\mathbf{Q}(t) = \begin{pmatrix} a_{0,0}(t) & a_{0,1}(t) & \ldots & a_{0,n}(t) \\ a_{1,0}(t) & a_{1,1}(t) & \ldots & a_{1,n}(t) \\ \vdots & \vdots & \vdots & \vdots \\ a_{n,1}(t) & a_{n,1}(t) & \ldots & a_{n,n}(t) \end{pmatrix} \tag{2}$$

where $a_{ij}(t)$ denotes the conversion rate between state i and state j. And the system evolution from initial state space $\mathbf{S}_0$ can be depicted as Eq. (3) with MRP:

$$\begin{aligned} \mathbf{P}'(t) &= \mathbf{P}(t)\mathbf{Q}(t) \\ \mathbf{P}(t=0) &= \mathbf{S}_0 \end{aligned} \tag{3}$$

As in Fig. 2, the performance of resilience begins when a disturbance happens in the system. Presuming the initial state space of the system to be $\mathbf{S}_0 = [1,0,\ldots,0]$. The system changes to a state of degradation after the disturbance. This can be represented by the change in the $\mathbf{P}(t)$ in Eq. (3). Set $a_{ij}(t) = \lambda_{ij}(t)$ to characterize the degradation of the system, where $\lambda(t)$ represents the failure rate. During the degradation of the system, it will receive remedies from the outside. $a_{ij}(t) = \mu_{ij}(t)$ is used to characterize the repair characteristics of the system, where $\mu(t)$ is the repair rate of the system.

3.1.2. Proposed resilience indices

The state transition map of the MSS, as part of the resilience assessment, is illustrated in Fig. 3. Corresponding to the vulnerable phase shown in Fig. 2, the system begins to degrade after experiencing a disturbance. It is assumed that the system starts from a normal operational state $\mathbf{S}_0$ and, after the disturbance, transitions forward into vulnerable states until it reaches the terminal state $\mathbf{S}_n$ (i.e., $\mathbf{S}_0 \rightarrow \mathbf{S}_n$). During this phase, the system's resistance and absorptivity to external disturbances are evaluated and quantified. When the system receives external remedies, the recovery phase is considered, during which the system undergoes a reverse transition process in the MRP (i.e., $\mathbf{S}_n \rightarrow \mathbf{S}_0$). This process evaluates the system's recovery capacity and rate. The duration the system spends in intermediary vulnerable states is considered as vulnerability.

Additionally, resilience is considered a global characteristic shaped by the system's historical state [44]. To capture this global resilience feature, concepts from calculus and cumulative probability have been integrated into the resilience assessment.

To further quantify the system's behavior during the processes described above, and to support comparisons of resilience characteristics across different systems as well as system structure optimization, a collection of resilience indices is proposed. This collection includes four indices: resistance, absorptivity, vulnerability, and recoverability. The definitions of these indices are provided below as **Definition.1-Definition.4** and depicted in Fig. 3.

Definition 1. (*Resistance*). The resistance in system resilience is defined as the capability of the system to maintain normal operational status after suffering from external disturbances, which can be denoted as:

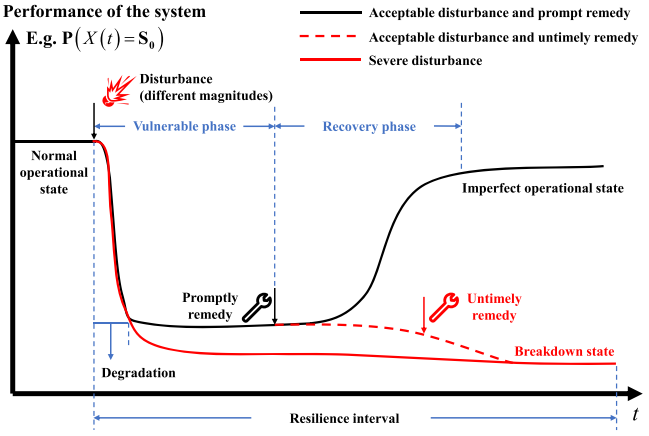

Fig. 2. System evolution curve based on MSS considering resilience interval

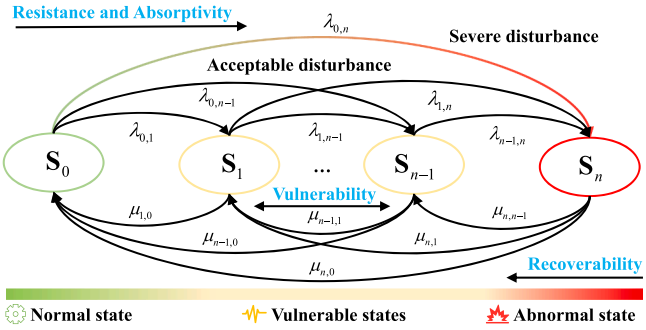

Fig. 3. Resilience state transition map of the system

$$\varphi_{\text{resist}} = \frac{1}{t_j - t_0} \int_{t_0}^{t_j} P(X(t) = S_0) dt \tag{4}$$

The φ_{resist} quantifies the probability of a system remaining in the S_0 state, from the moment t_0 when the system is disturbed ted until the current time t_j. To clearer analysis, this metric is made dimensionless and normalized, hence situating φ_{resist} within the range of $[0,1]$. Similar operations are also applied to the subsequent indices.

Definition 2. (*Absorptivity*). The absorptivity in system resilience is defined as the ability of a system to maintain partial functionality and prevent breakdown. It can be denoted as:

$$\varphi_{\text{a}} = \frac{1}{t_j - t_0} \int_{t_0}^{t_j} [1 - P(X(t) = S_n)] dt \tag{5}$$

The φ_{a} quantifies the probability of a system remaining in the state space $\mathbf{S}' = \{0, \ldots, n-1\}$ from t_0 to t_j. A higher absorptivity implies that under equivalent disturbance, the system affords a longer buffering period until the remedy.

Definition 3. (*Vulnerability*). The vulnerability in system resilience is defined as the possibility of the system becoming unstable after being disrupted. Herein, the vulnerable states mean that the system cannot work normally yet it hasn't completely failed. It can be denoted as:

$$\varphi_{\text{v}} = \frac{1}{t_j - t_0} \int_{t_0}^{t_j} [1 - P(X(t) = S_0) - P(X(t) = S_n)] dt \tag{6}$$

The φ_{v} quantifies the probability of a system remaining in the state space $\mathbf{S}'' = \{1, \ldots, n-1\}$ from t_0 to t_j. When a system remains in an unstable state for a relatively long time, there is a higher probability that it will eventually transition into breakdown.

Definition 4. (*Recoverability*). Recoverability in system resilience is defined as the possibility of a system quickly recovering from breakdown and vulnerable states. Since recovery should be time-sensitive [45], the cost of recovery is introduced to reflect the increased degradation and higher repair costs as the system remains longer in the vulnerable stage. Modeling these costs provides a more accurate assessment of the recovery rate and clarifies the trade-offs in system resilience. By including recovery costs in resilience assessments, both recovery speed and associated costs are considered [46], offering a more comprehensive evaluation. Consequently, recoverability introduces the recovery rate as an additional factor, with the cost of recovery rising rapidly as the vulnerable stage persists. An exponential function is used to describe the time-dependent change in the costs, as expressed in Eq. (7).

$$C(t) = e^{\eta\left(1 - \frac{t_0}{t_n}\right)} \tag{7}$$

where η is the shape parameter. A greater η indicates an inferior feature for the recovery cost in the system. Based on this, the recoverability of the system can be articulated as:

$$\varphi_{\text{recover}} = \frac{1}{C(t)(t_j - t_0)} \int_{t_0}^{t_j} \left[1 - \sum_{k=1}^{n-1} P\left(X(t) = S_k \middle|_{\mu_{k,0}>0}\right)\right] dt \tag{8}$$

where k denotes the states with positive repairing rate to health states in $\mathbf{S}''$ from t_0 to t_j. The φ_{recover} focus on the probability of the system remaining in state space $\mathbf{S}''$. Overall, the $\boldsymbol{\varphi}_{\text{t}} = [\varphi_{\text{resist}}, \varphi_a, \varphi_v, \varphi_{\text{recover}}]$ is used as the resilience collective in the following description.

3.2. PINN for MSS resilience assessment

The precise and effective solution for state transition is crucial for the resilience assessment with MSS. This subsection presents a comprehensive introduction to the effective MRP solver based on PINNs. As shown in Fig. 4, the solver consists of two steps. In the first step, a neural network model is constructed. The loss function is established based on the governing equations and the initial state of the MRP. The second step deals with the drawbacks of the gradient direction caused by the nature of multi-project training for neural networks. This is accomplished by implementing an effective neural network training method.

3.2.1. PINN modelling

A PINN for MSS resilience assessment, governed by the ODE (i.e., Eq. (3)), initiates with the establishment of a Deep Neural Network (DNN). It serves as a surrogate for the ODE solution. The FNN is employed in this case. It's relatively simple, but sufficient for most ODE solving problems with PINN. As shown in Fig. 4, the training of the FNN encompasses a two-fold process: forward propagation and back propagation.

In the forward propagation, the temporal variables denoted as t are introduced as input, and the solution $\widehat{\boldsymbol{\Phi}}(t;\boldsymbol{\theta}) = [\mathbf{P}_i(t;\boldsymbol{\theta})]$ as output. Here, $\boldsymbol{\theta}$ denotes a vector that holds the weights and biases of all neurons. The fine-tuning for $\boldsymbol{\theta}$ with a gradient descent algorithm is executed during back propagation. The variables denoted with a hat symbolize $\widehat{\boldsymbol{\Phi}}$ those computed by the neural network. The next key step is to constrain the output $\widehat{\boldsymbol{\Phi}}(t;\boldsymbol{\theta})$ to satisfy the physical laws defined by Eq. (3). To quantify the compliance of the neural network with the physical laws, the residuals are defined as:

$$F_1 = \widehat{P}(t=0) - S_0 \tag{9}$$

$$F_2 = \frac{d\widehat{\mathbf{P}}_i(t)}{dt} - \mathbf{P}_i(t) \cdot \mathbf{Q}(t) \tag{10}$$

The residual vector $\mathbf{F} = [F_1, F_2]$ signifies the degree to which the PINN conforms to physical laws in MRP.

Smaller residual values indicate higher conformity. The time derivatives $\frac{d\widehat{\mathbf{P}}_i(t)}{dt}$ in F_2 are computed utilizing the AD algorithm. Notably, AD can precisely compute the derivative of numeric functions expressed as a graph structure, particularly in the case of neural networks. It obviates the need for approximation schemes (e.g., the finite difference approximation), and bypasses errors such as truncation and rounding. Consequently, the PINN is a mesh-free method, negating the need for a discrete mesh in solving the ODEs. Based on the description above, the loss function $L(\theta)$ in the PINN is constructed by:

$$L(\boldsymbol{\theta}) = F_1^2(t_j;\boldsymbol{\theta}) + \frac{1}{N} \sum_{j=1}^{N} \left(F_2^2(t_j;\boldsymbol{\theta})\right) \tag{11}$$

where N indicates the number of the samples of time.

Subsequently, in the backward-propagation phase, the gradients of the $L(\boldsymbol{\theta})$ are calculated using the back propagation rules as:

$$\Delta_0 = \frac{\partial}{\partial \boldsymbol{\theta}} L(\widehat{P}(t=0) - S_0;\boldsymbol{\theta}) \tag{12}$$

$$\Delta_i = \frac{\partial}{\partial \boldsymbol{\theta}} L\left(\frac{d\widehat{\mathbf{P}}_i(t)}{dt} - \mathbf{P}_i(t) \cdot \mathbf{Q}(t);\boldsymbol{\theta}\right) \tag{13}$$

where Δ_0 denotes the gradients combined with the initial state equation and Δ_i denotes the gradients calculated from the state transition equation at $\mathbf{S}_i$. The $\boldsymbol{\theta}$ is iteratively updated through this process on the whole training samples until the total loss converges. In addition, the convergence of the total loss function, in this paper, is evaluated by the

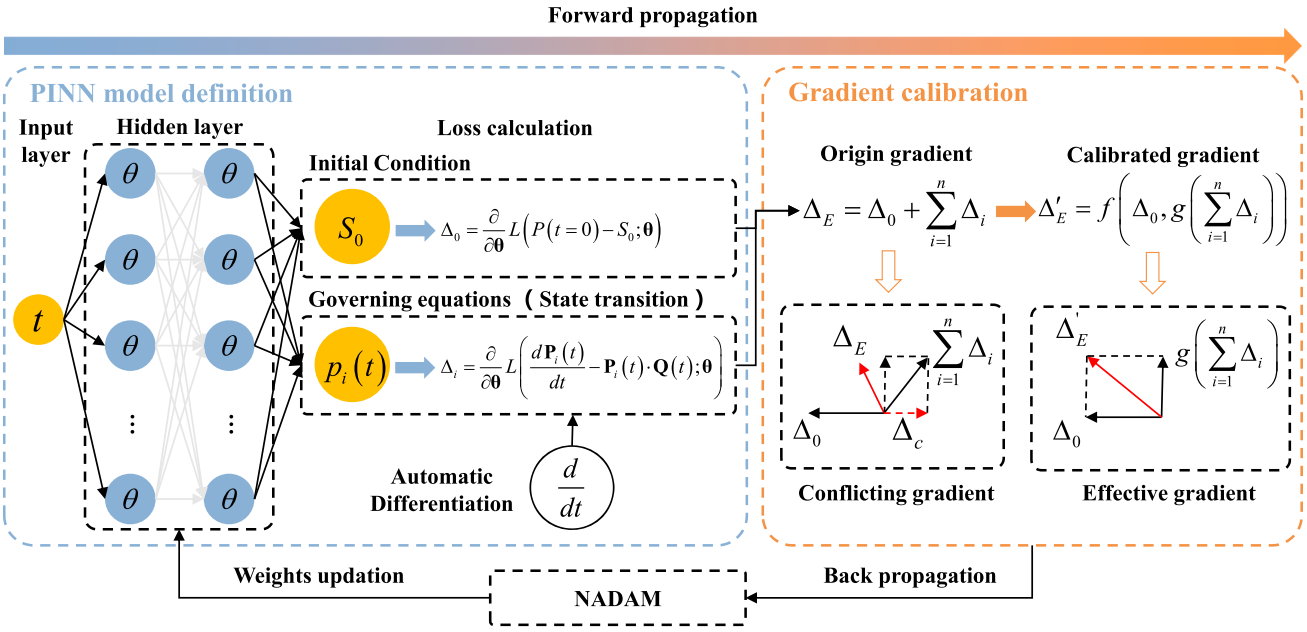

Fig. 4. Flowchart of the PINN modeling for MRP with MSS

Nesterov-accelerated Adaptive Moment Estimation (NADAM) algorithm [47]. It combines the benefits of two popular methods, Root Mean Square Propagation (RMSProp) and Adaptive Moment Estimation (ADAM). Besides, it incorporates Nesterov Accelerated Gradient (NAG) into ADAM. Nesterov acceleration is a technique used to speed up gradient descent. It achieves this by starting at the current training sample and jumping ahead reasonably by the momentum. NADAM is robust to changes in hyperparameters and avoids local minima, resulting in the speeding of model training.

3.2.2. *Gradient calibration for stable solution with resilience assessment*

Investigating Eqs. (12) and (13), it is apparent that the units of Δ_0 and $\Delta_s = \sum_{i=1}^{n} \Delta_i$ are inconsistent. This discrepancy leads to a ubiquitous issue within PINNs: the magnitudes of the gradient vectors corresponding to each loss function differ substantially. If these two gradient vectors conflict in direction (i.e., the cosine similarity of the two vectors is less than 0), it may result in the neural network parameters' training relying solely on one of the gradient vectors. This conflict is indicated in the original gradient calculation part in Fig. 4. Consequently, the trained neural network fails to provide accurate results with lower convergence. To address this issue [40,43], proposed a gradient calibration method for these conflict losses in training. The core of this method involves calibrating one of the gradients when two gradient vectors conflict. For another gradient Δ_0, the conflicting component of gradient $\sum_{i=1}^{n} \Delta_i$, denoted as Δ_c, is treated as zero. Then, the calibrated gradient is:

$$\Delta'_s = \Delta_0 - \frac{\Delta_0 \cdot \Delta_s}{\| \Delta_0 \| \| \Delta_s \|} \Delta_s \tag{14}$$

After such calibration, both gradient vectors Δ_0 and Δ'_s can provide useful information for neural network training, thereby avoiding gradient masking. The overall calibrated gradient Δ'_E is then obtained through vector addition.

4. Numerical example

4.1. *Experimental setup*

Assuming a MSS with multiple units, it exists certain units that play a more crucial role in ensuring the normal functionality of the entire system. Once those units fail, the system will breakdown and give out with low acceptance to external disturbance. In such cases, there are two methods to enhance those MSS with resilience: (1) ensuring high reliability of the core units. This approach incurs high maintenance costs. (2) Implementing a redundant design, such as introducing one or more parallel protective units. This redundant approach, i.e., standby, significantly increases the probability of the unit continuing to work properly when subjected to external disturbance.

As a result, the standby structure is widely used in MSS, for example, in gas pressure boosting devices [4], hydrogen supply devices [5], and the operational core of nuclear power plants [30]. However, factors such as the natural degradation of standby units, and the probability of normal startup of standby units can affect the ability of the standby system. These influences need further quantification and discussion under resilience. Therefore, the numerical example of this study focuses on various redundant structures on MSS. The proposed resilience assessment method is used.

4.1.1. *Description of the standby structures in MSS*

Most complex standby structures can be simplified into two parallel units. Therefore, this study primarily focuses on the analysis of the two-unit standby structure. As shown in Fig. 5, *S* represents the system switch cell, *A* represents the normal operational unit of the system at the initial state, and $B(A')$represents the standby unit of the system. Under both normal degradation and external disturbance, the failure rate of the unit i is denoted by $\lambda_i (i = A,B)$. When the active unit fails, it immediately is under repair. The repair rate follows an exponential distribution with a parameter of $\mu_i (i = A,B)$. Once the unit is repaired, it immediately goes into a standby state.

The standby in the system, the successful upload, and the natural degradation in standby units are being considered. There are systems with four structures being discussed as follows:

- **System I** (*Cold storage and perfect switch*). As shown in Fig. 5 (a), considering the passivity of the standby unit, it is assumed that failure will not occur during its standby phase. The switch is presumed perfect. Furthermore, it is assumed that any failure in the active unit would be immediately detected. The successful activation of the standby unit is a certainty.
- **System II** (*Cold storage and perfect switch, Unit A as the main working unit*). Based on **System I**, unit *A* is set as the primary working unit.

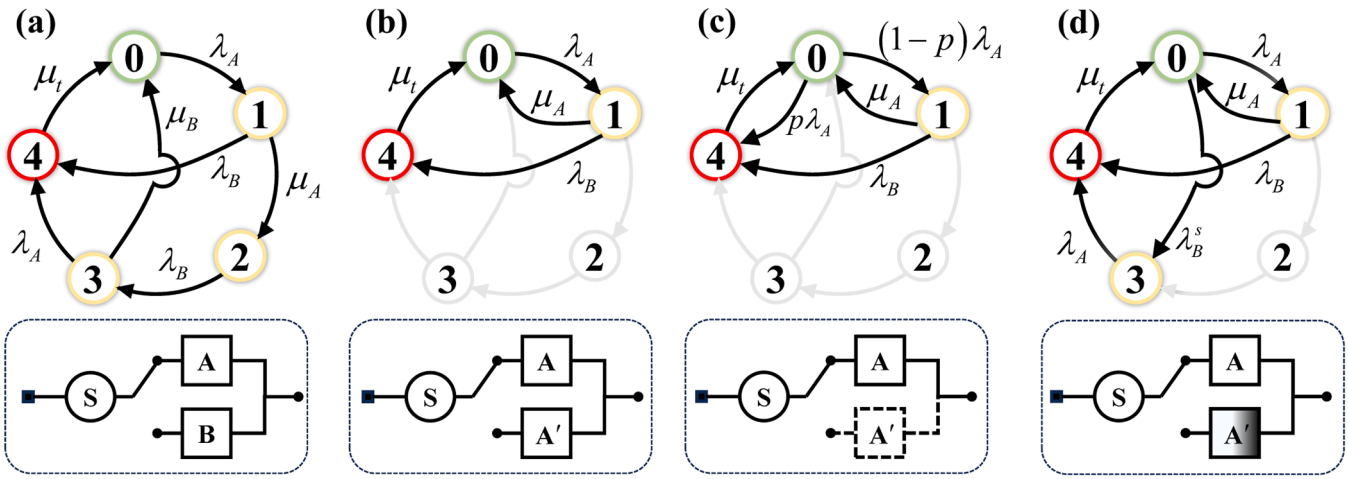

Fig. 5. System state transition for MSS with a redundant structure. (a). Cold storage and perfect switch. (b). Cold storage and perfect switch, unit A as the main working unit. **(c)**. Cold storage and non-perfect switch, unit A as the main working unit. **(d)**. Partial load standby, perfect switch, and unit A as the main working unit.

Unit B is only used when Unit A fails or requires maintenance. As illustrated in Fig. 5 (b), once unit A is able to function properly, unit B automatically switches to a standby state. The system is considered to be in a breakdown only when unit B fails and unit A is being repaired simultaneously

- **System III** (*Cold storage and non-perfect switch, Unit A as the main working unit*). According to Fig. 5 (c), based on **System II**, it is assumed that the switch is not perfectly toggled. When the active unit A fails, the standby unit B will activate with a probability of $(1-p)$.
- **System IV** (*Partial load standby, perfect switch, and Unit A as the main working unit*). According to **System II**, and based on Fig. 5 (d), it is assumed that the standby unit B may fail during the standby period. Let the failure rate be denoted as λ_B^s. It can be considered smaller than λ_B.

Therefore, the possible states that the MSS with standby can be in are summarized in Table 2.

Based on the previous description, it is assumed that each system has a common maintenance rate λ_i and degradation rate μ_i. The state transition rate matrix **Q** for each system and the assumed value used in subsequent experiments are shown in Table 3.

4.1.2. Guidelines for network training

The PINN training steps for MRP solver in resilience assessment are shown in Fig. 6. After time-space discretization and sampling for the input points, the samples are randomly divided into two parts, the training samples and validation samples. The trained PINN has extrapolation capabilities [48]. The sampling of training and validation points does not overlap. The training points used for network weights optimization are divided into several batches, successively provided for an epoch of training updates. Determining the number of training epochs is critical for neural network learning. A validation point set with 20 % of the data is used for an early stop mechanism [49]: when the loss function of the model cannot be improved by $\Delta_{\min}$ within 3000 training epochs, which is called patience, the training process is terminated.

The architecture of the neural network is based on FNN. Each of the three hidden layers consists of 80 neurons and applies the tanh activation function. The number of neurons in the output layer matches the number of states n in the target MSS under MRP. Additionally, L2 regularization [50] and Dropout [51] mechanisms are introduced in the hidden layers to mitigate overfitting during the training process.

For initial details in model training, the learning rate is set to 0.001 and NADAM is used as the optimizer for automatically adjust and compute the learning rate at each step of the training process. The batch size is set to 512. The code runs in Python 3.9 with TensorFlow 2.9.1 frameworks. As a summary, the default training hyperparameters of the model are given in Table 4. They have been set by a grid search mechanism [52].

For a given time space T_0, the predictions of the trained PINN model are compared with the exact solution from the eigenvector method. The root mean square error (RMSE) is used as the accuracy matric in Eq. (15).

Table 2
Status of the Parallel Standby system

System State	State of Unit A	State of Unit B
0	S_w	S_b
1	S_f	S_w
2	S_b	S_w
3	S_w	S_f
4	S_F	S_f

S_w means the normal operational state, S_b means the standby state, S_f means the failure state.

Table 3
Calculation parameters for each system

System index	State transition rate matrix	Key value of the system
I	$\mathbf{Q}_{\mathrm{I}} = \begin{pmatrix} -\lambda_A & \lambda_A & 0 & 0 & 0 \\ 0 & -(\lambda_B+\mu_A) & \mu_A & 0 & \lambda_B \\ 0 & 0 & -\lambda_B & \lambda_B & 0 \\ \mu_B & 0 & 0 & -(\lambda_A+\mu_B) & \lambda_A \\ \mu_t & 0 & 0 & 0 & -\mu_t \end{pmatrix}$	$\lambda_A = 2.3\times 10^{-4}\mathrm{h}^{-1}$, $\lambda_B = 1.7\times 10^{-4}\mathrm{h}^{-1}$, $\lambda_B^s = 8.5\times 10^{-5}\mathrm{h}^{-1}$, $\mu_A = 8.3\times 10^{-2}\mathrm{h}^{-1}$, $\mu_B = 4.2\times 10^{-2}\mathrm{h}^{-1}$, $\mu_t = \mu_A + \mu_B = 1.25\times 10^{-1}\mathrm{h}^{-1}$, $p = 0.05$
II	$\mathbf{Q}_{\mathrm{II}} = \begin{pmatrix} -\lambda_A & \lambda_A & 0 & 0 & 0 \\ \mu_A & -(\lambda_B+\mu_A) & 0 & 0 & \lambda_B \\ 0 & 0 & 0 & 0 & 0 \\ 0 & 0 & 0 & 0 & 0 \\ \mu_t & 0 & 0 & 0 & -\mu_t \end{pmatrix}$	
III	$\mathbf{Q}_{\mathrm{III}} = \begin{pmatrix} -\lambda_A & (1-p)\lambda_A & 0 & 0 & p\lambda_A \\ \mu_A & -(\lambda_B+\mu_A) & 0 & 0 & \lambda_B \\ 0 & 0 & 0 & 0 & 0 \\ 0 & 0 & 0 & 0 & 0 \\ \mu_t & 0 & 0 & 0 & -\mu_t \end{pmatrix}$	
IV	$\mathbf{Q}_{\mathrm{IV}} = \begin{pmatrix} -(\lambda_A+\lambda_B^s) & \lambda_A & 0 & \lambda_B^s & 0 \\ \mu_A & -(\lambda_B+\mu_A) & 0 & 0 & \lambda_B \\ 0 & 0 & 0 & 0 & 0 \\ 0 & 0 & 0 & -\lambda_A & \lambda_A \\ \mu_t & 0 & 0 & 0 & -\mu_t \end{pmatrix}$	

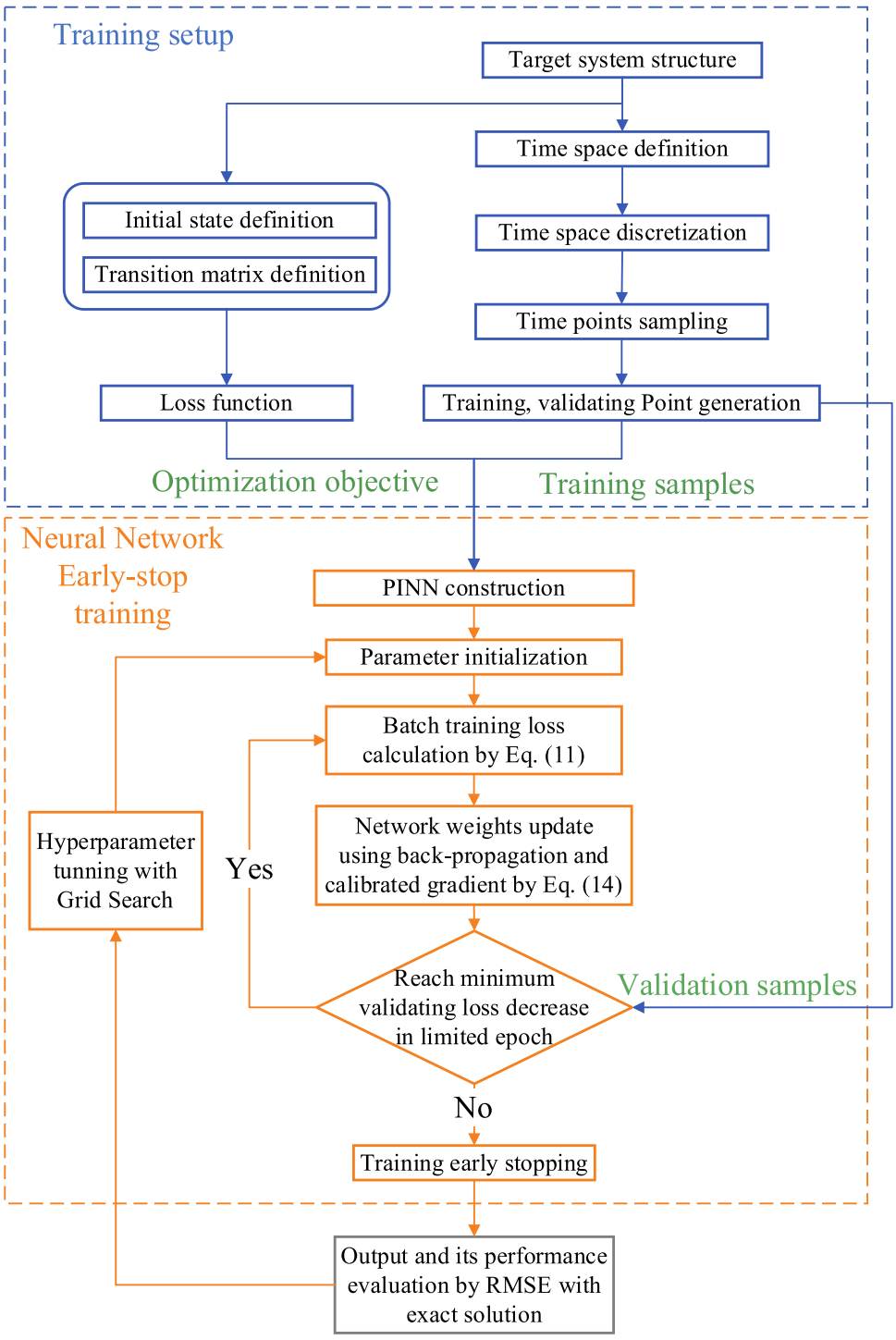

Fig. 6. Flowchart of the PINN training

Table 4
Default training hyperparameter

Hyperparameter	Default Value
Optimizer	NADAM
Learning rate	0.001
Patience	3000
Δ_{min}	1×10^{-13}
Training set proportion	0.8
Batch size	512

$$RMSE = \frac{1}{n}\sum_{j=0}^{n}\sqrt{\frac{1}{N}\sum_{i}^{N}\left(P_t - P_{tp}\right)^2} \tag{15}$$

where n denotes the count of the states in Fig. 5, N denotes the number of samples in the time space T_0, P_t denotes the true value of the state's probability, and P_{tp} denotes the estimations.

4.2. Results and analysis

4.2.1. Network training and comparation

Herein, the precise solution provided by the PINN serves as the foundation for the proposed resilience assessment method. Therefore, the PINN is trained using the basic parameters listed in Tables 3 and 4, and four different MSS with standby are tested accordingly. Additionally, the gradient calibration method proposed in Section 3.2.2 is verified.

To demonstrate the effectiveness of the proposed gradient calibration method for PINN, both the original and improved PINNs are tested with the same number of training epochs (10,000). The results, as depicted in Fig. 7, show that while the original PINN failed to converge in certain systems, the improved method with gradient correction consistently achieved convergence across all systems, with losses reduced to less than 10^{-11} [40,53]. This indicates that the proposed approach significantly enhances the stability and efficiency of PINN training for complex multi-state systems.

The PINN training with gradient calibration not only converges faster but also exhibits a relatively stable training process. This stability is crucial, especially when considering the fluctuations introduced by the NADAM optimizer during training. Although the loss function with gradient calibration shows some local fluctuations instead of a consistently smooth decrease, this behavior is expected due to the momentum incorporated in NADAM's gradient descent process. While this can occasionally lead to suboptimal training directions, the use of momentum is essential for improving the robustness of the model's convergence. NADAM's ability to prevent the model from becoming trapped in local minima ultimately ensures that the final training outcome is more robust and globally optimal.

The computational cost of PINN was compared with that of the eigenvector method to highlight its efficiency. In the eigenvector method, each point in the state space must be solved sequentially, leading to significant computational expenses as the complexity of the system increases. In contrast, PINN requires only a partial sampling of points for training. Once trained, PINN can estimate the entire time-space efficiently.

As illustrated in Fig. 8, as the number of samples increases, the computational cost of the traditional eigenvector method escalates significantly, while PINN maintains a consistently lower computational load. Unlike traditional numerical or analytical methods, PINN, after its initial training, can rapidly provide solutions for MRP. Notably, when the number of samples reaches 4×10^7, PINN can reduce the computational cost by 92.4 % compared to the eigenvector method. This significant reduction in computational cost demonstrates the practical advantages of using PINNs, particularly in scenarios where efficiency and scalability are critical. Thus, the choice of PINNs is not only justified but also essential for handling complex multi-state systems effectively.

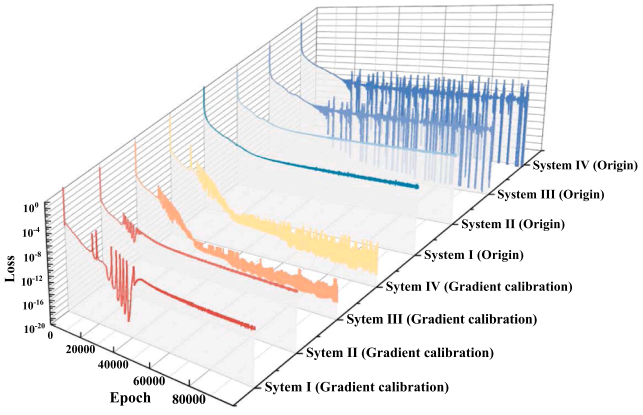

Fig. 7. Comparation of PINN training with and without gradient calibration

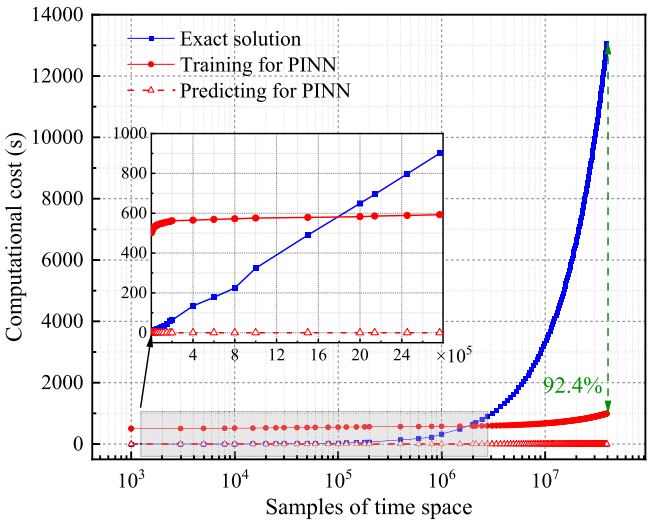

Fig. 8. Computation cost between PINN and exact solution

To validate the accuracy of the PINN further, the trained PINN model is tested with four systems. The results are compared with the exact solutions in Fig. 9. To illustrate informatively, both the results from PINN and the exact solutions for MRP transition probability matrix $\mathbf{P}(\mathbf{X}(t))$ are plotted as the X-axis and Y-axis, respectively. It combines all of the errors under all state space $\mathbf{S}$. When the estimation lies on the diagonal depicted by the black dash line, this indicates the accuracy of the PINN solution. Among all the estimations, the largest deviation by PINN is about 3.68×10^{-5}.

Generally, most of the deviation of PINN is centered on the small probability range. It is attributed to the slack variables ε in the training process to prevent gradient explosion [54]. The magnitude of ε is usually in $\left[10^{-11}, 10^{-8}\right]$. This makes the neural network training extremely sensitive to very small probability values. Furthermore, the RMSE of PINN is computed with **Eq. (19)**, as demonstrated in Table 5. The overall error is within an acceptable range.

To clarify the scalability of our framework, we define the system's size in terms of the state transition phases. In engineering applications, an increase in the number of states leads to a more sparse state transition matrix and a larger matrix size. In this study, we have selected four basic configurations of standby systems to evaluate computational efficiency. Larger systems with more state transitions can be understood as

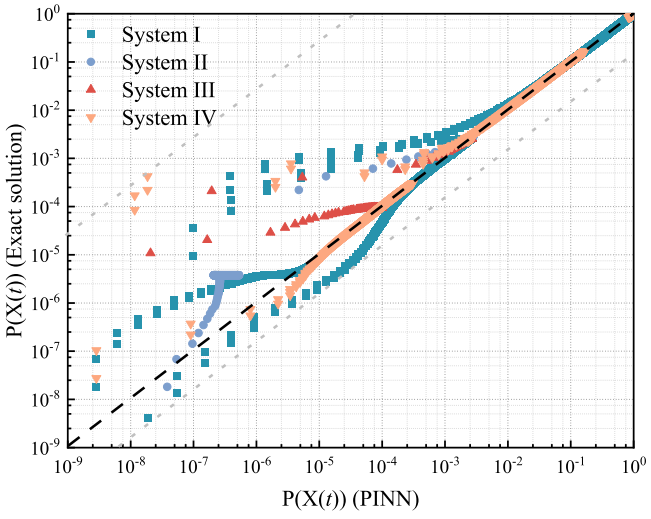

Fig. 9. Comparation between PINN and exact solution for process evolution with the setting systems

Table 5
RMSE for the solution on the setting system with PINN

System index	RMSE
I	1.15×10^{-3}
II	8.41×10^{-5}
III	1.54×10^{-4}
IV	2.59×10^{-4}

combinations of these four standby modes. Additionally, the use of GPU acceleration has proven to significantly enhance the performance of the PINN, making it possible to efficiently handle larger and more complex systems. Therefore, in the subsequent modeling and analysis of resilience assessment for MSS with standby, the PINN trained with gradient calibration is adopted to ensure both computational efficiency and accuracy.

4.2.2. *Effect of structure in MSS with standby for resilience*

Based on the resilience indices proposed in Section 3.1.2, the changes in resilience collection $\boldsymbol{\varphi}_t$ for the four systems are calculated, as shown in Fig. 10. For a standby system, such as systems II, III, and IV, when the system uses a certain unit as the primary working unit, the system has stronger resistance (i.e., higher φ_{resist}) and tends to keep in normal operation. When the standby units have degradation characteristics, such as System IV, the system's resistance will decline, and the system will become more vulnerable. Observing Systems III and IV, it can be found that the abnormal switch and degradation of standby can reduce the system's absorptivity. The recoverability of the four systems all decrease to a lower level over time. Therefore, adopting a standby for MSS, or methods to improve the standby behavior, will hardly significantly enhance the system's recoverability.

In general, by adopting a standby for the MSS, the resistance can be effectively enhanced, and the resilience of the system during the vulnerable phase can be strengthened. However, it is still necessary to enhance the system's recoverability from the perspective of improving the overall recovery rate μ of the system.

4.2.3. *Effect of balance between failure and repair rate in MSS with standby*

As described in Section 3.2.1, optimizing the structure of the MSS mainly affects its resilience in the vulnerable phase. The combination of the failure rate and the repair rate is another perspective of resilience enhancement in MSS with standby. Therefore, a joint analysis of the ratio of failure rate and repair rate $\frac{\lambda}{\mu}$ with the system's resilience indices is carried out. The system's failure rate λ is set as a constant in Table 3.

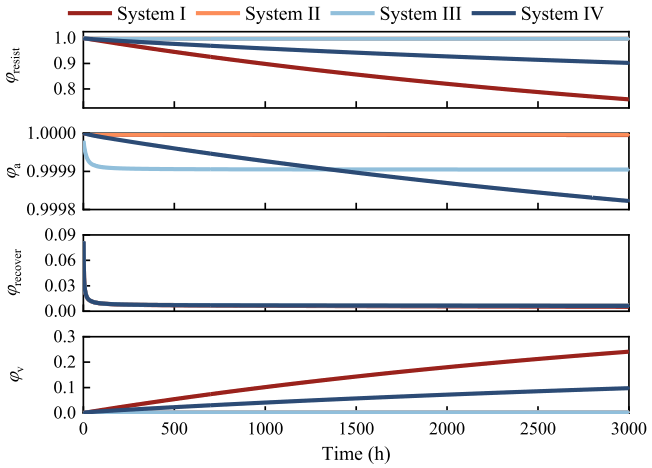

Fig. 10. Resilience indices for evolution with the setting systems

Let the μ changes, the system's repair rate μ is multiplied by a conversion factor α, forming a new repair rate $\mu_g = \mu \times \alpha$. When the dimension level difference is 10^2, the μ_g and λ are considered much greater or much less than each other. Therefore, the conversion factor α is continuously increased from 0.001 to 100, with a step of 0.05. It is well known that a MRP eventually reaches a steady state. The resilience indices have been integrated the transient factors of the MRP into the modeling using calculus. To assess the overall resilience of different standby systems comprehensively, the resilience collection $\boldsymbol{\varphi}_t$ at steady-state is used. This allows for comparative analysis across all phases, from disturbance to recovery.

As shown in Fig. 11, when the repair rate μ_g is a very low value (i.e. α is a low value), the overall resilience indices of all systems are also in a lower state. With the increase of μ_g, the resilience indices of System II and System III develop towards a better direction at the fastest rate. Therefore, adopting the structure with a certain unit as the main one can significantly enhance the effects of external remedies received by the system. When μ_g reaches a large enough value, that is, the system receives the timeliest remedial measures, the simple parallel work unit may still fail. But by adopting a working mode with a certain unit as the main one, it can enhance and even perfectly guarantee the normal operation of the system. The case in which standby units with abnormal switch does not significantly affect the resilience of the system. By contrast, the natural degradation of the standby will reduce the effect of system repair. When the system's repair rate is at an average level (i.e., $\lambda \approx \mu_g$), and the health of standby cannot be guaranteed, the standby structure is not working well in the vulnerable stage. It only enhances resilience during the recovery phase.

As a result, adopting a standby system and ensuring the health of standby is core to improving the overall resilience of the parallel working MSS. This will enable the system to absorb external disturbances effectively with the same level of remedies.

5. Conclusion

In this paper, a resilience assessment framework for MSS under MRP is proposed. The resilience interval is divided into vulnerable and recovery phases. Based on these phases, a resilience indices collection is derived, from the perspective of cumulative evolution of the system. An effective solver for MRP is proposed based on enhanced PINN.

The resilience analysis conducted in this study provides insights that extend beyond those offered by traditional reliability analysis. While reliability analysis primarily assesses the likelihood of system failure, resilience analysis considers the system's overall response to disturbances, including its capacity to absorb disturbances and recover towards a normal operational state. The resilience indices—resistance, absorptivity, vulnerability, and recoverability—offer a detailed assessment of the system's performance throughout the different phases of disturbance and recovery. This comprehensive approach supports more informed decision-making for improving system robustness and recovery strategies, especially for critical infrastructures facing high-impact events.

In the vulnerability stage, three indices are proposed: resistance, absorptivity, and vulnerability. These indices focus on ensuring normal operation, preventing complete system breakdown, and controlling system vulnerability, respectively. Moreover, recoverability is proposed considering recovery costs a long time during the recovery phase. The proposed resilience assessment method is applied to analyze a typical parallel multi-state system (MSS). The results indicate that for a two-unit parallel structure, using one unit as the main working unit or relying on a standby system can enhance the system's resilience during vulnerable phases.

For an effective MRP solution, the introduction of PINN can reduce the computational cost by 92.4 % with 4×10^7 time samples compared to the eigenvector method. The RMSE is at an average level of $2.59 \times$

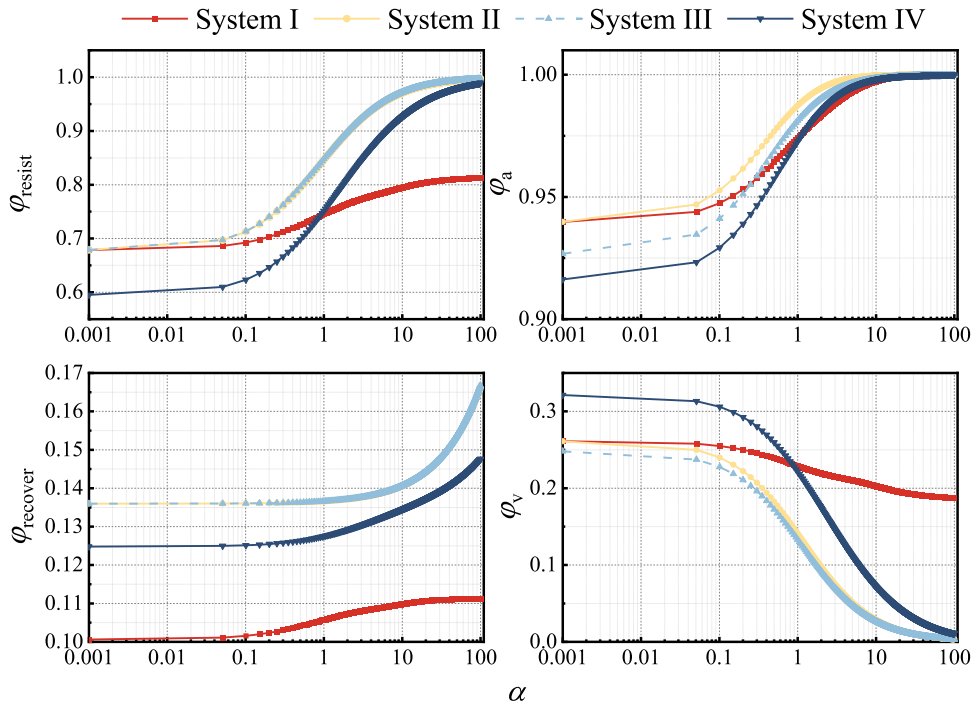

Fig. 11. Resilience indices for the setting systems at steady-states with rate between μ and λ

10^{-4}. For PINN training, the imbalance caused by loss magnitudes is the critical factor that leads to non-convergence and affects the training efficiency. The proposed training method provides a means for the stable convergence of PINN with MRP. The gradient calibration balances multiple training losses of PINN by transforming the vectors of conflicting loss. It gives orthogonality to the loss gradient and accelerates the convergence of the training neural network during backpropagation with NADAM. Although this approach introduces more significant fluctuations in the training process, it effectively reduces the complexity of parameter tuning and the possibility of failure during training. In resilience assessment under MSS, it is essential to solve MRPs that involve extremely rare probability values. These small probability values can still bring gradient explosion to the PINN training.

In future work, the following aspects can be focused on three key points:

- Although the trained PINN can achieve efficient response, the training process of PINN is still slow and uncertain. The solution for PINN training in this paper still relies on a large volume of parameter tuning. The training process of PINN needs to be more intelligent and automated to speed up training and convergence to reduce computational cost.
- For the analysis of resilient systems, this paper only considers the classical parallel system under a two-unit configuration. In practical systems, there may exist series, mixed, or even more complex system structures. Further exploration, modeling, and validation for the resilience of these structures are needed.
- The physics mentioned in this paper is based on the quantification of system transitions between different stages in the MRP. In practical applications, the failure rates λ and repair rates μ within the state transition matrix exhibit more complex physics, which has been simplified through assumptions in this study. Future research should focus on developing more scientifically rigorous quantification methods, such as those based on fault tree analysis and related techniques.

CRediT authorship contribution statement

Yuxuan He: Writing – review & editing, Writing – original draft, Software, Methodology, Conceptualization. **Enrico Zio:** Writing – review & editing, Methodology. **Zhaoming Yang:** Software, Data curation. **Qi Xiang:** Writing – original draft, Visualization. **Lin Fan:** Software, Data curation. **Qian He:** Writing – original draft, Visualization. **Shiliang Peng:** Writing – original draft, Visualization. **Zongjie Zhang:** Methodology. **Huai Su:** Visualization. **Jinjun Zhang:** Supervision, Funding acquisition.

Declaration of competing interest

The authors declare that they have no known competing financial interests or personal relationships that could have appeared to influence the work reported in this paper.

Acknowledgment

This work is supported by National Natural Science Foundation of China [grant number 51904316], and the research fund provided by China University of Petroleum, Beijing [grant number 2462021YJRC013, 2462018YJRC038].

Data availability

Data will be made available on request.

References

[1] Soomro AA, Mokhtar AA, Kurnia JC, Lashari N, Lu H, Sambo C. Integrity assessment of corroded oil and gas pipelines using machine learning: a systematic review. Eng Fail Anal 2022;131:105810. https://doi.org/10.1016/j.engfailanal.2021.105810.
[2] Zio E. Reliability engineering: old problems and new challenges. Reliab Eng Syst Safe 2009;94:125–41. https://doi.org/10.1016/j.ress.2008.06.002.
[3] Paltrinieri N, Øien K, Cozzani V. Assessment and comparison of two early warning indicator methods in the perspective of prevention of atypical accident scenarios. Reliab Eng Syst Safe 2018;108:21–31. https://doi.org/10.1016/j.ress.2012.06.017.

[4] Fan L, Su H, Zio E, Li Y, Zhang L, Peng S, He Y, Hao Y, Zhang J. Supply reliability-driven joint optimization of maintenance and spare parts inventory in a gas pipeline system. Gas Sci Eng 2023;110:204883. https://doi.org/10.1016/j.jgsce.2023.204883.

[5] Shen Y, Lv H, Hu Y, Li J, Lan H, Zhang C. Preliminary hazard identification for qualitative risk assessment on onboard hydrogen storage and supply systems of hydrogen fuel cell vehicles. Renew Energ 2023;212:834–54. https://doi.org/10.1016/j.renene.2023.05.037.

[6] Wang Y, Zhao O, Zhang L. Multiplex networks in resilience modeling of critical infrastructure systems: A systematic review. Reliab Eng Syst Safe 2024;250:110300. https://doi.org/10.1016/j.ress.2024.110300.

[7] Nogal M, O'Connor A, Caulfield B, Martinez-Pastor B. Resilience of traffic networks: from perturbation to recovery via a dynamic restricted equilibrium model. Reliab Eng Syst Safe 2016;156:84–96. https://doi.org/10.1016/j.ress.2016.07.020.

[8] Das L, Munikoti S, Natarajan B, Srinivasan B. Measuring smart grid resilience: methods, challenges and opportunities. Renew Sust Energy Rev 2020;130:109918. https://doi.org/10.1016/j.rser.2020.109918.

[9] Hossain E, Roy S, Mohammad N, Nawar N, Dipta DR. Metrics and enhancement strategies for grid resilience and reliability during natural disasters. Appl Energ 2021;290:116709. https://doi.org/10.1016/j.apenergy.2021.116709.

[10] Carvalho PV, Dos Santos IL, Gomes JO, Borges MR. Micro incident analysis framework to assess safety and resilience in the operation of safe critical systems: a case study in a nuclear power plant. J Loss Prevent Proc 2008;21:277–86. https://doi.org/10.1016/j.jlp.2007.04.005.

[11] Sun H, Yang M, Zio E, Li X, Lin X, Huang X, Wu Q. A simulation-based approach for resilience assessment of process system: a case of LNG terminal system. Reliab Eng Syst Safe 2024;249:110207. https://doi.org/10.1016/j.ress.2024.110207.

[12] Trivedi KS, Vaidyanathan K, Selvamuthu D. Markov chain models and applications. Elsevier 2015:393–421. https://doi.org/10.1016/B978-0-12-800887-4.00013-4.

[13] Soares CG. Evaluation of the availability and reliability of a standby repairable system valuation of the availability and reliability of a standby repairable system incorporating imperfect switchovers and working breakdowns. Reliab Eng Syst Safe 2018;180:1. https://doi.org/10.1016/j.ress.2020.107366.

[14] Abba B, Wu J, Muhammad M. A robust multi-risk model and its reliability relevance: a Bayes study with Hamiltonian Monte Carlo methodology. Reliab Eng Syst Safe 2024;250:110310. https://doi.org/10.1016/j.ress.2024.110310.

[15] Mehni MB, Mehni MB. Reliability analysis with cross-entropy based adaptive Markov chain importance sampling and control variates. Reliab Eng Syst Safe 2023;231:109014. https://doi.org/10.1016/j.ress.2022.109014.

[16] Cuomo S, Di Cola VS, Giampaolo F, Rozza G, Raissi M, Piccialli F. Scientific machine learning through physics–informed neural networks: where we are and what's next. J Sci Comput 2022;92:88. https://doi.org/10.1007/s10915-022-01939-z.

[17] Holling CS. Resilience and stability of ecological systems. 1973. https://doi.org/10.1017/9781009177856.038.

[18] Hosseini S, Barker K, Ramirez-Marquez JE. A review of definitions and measures of system resilience. Reliab Eng Syst Safe 2016;145:47–61. https://doi.org/10.1016/j.ress.2015.08.006.

[19] Bruneau M, Chang SE, Eguchi RT, Lee GC, O'Rourke TD, Reinhorn AM, Shinozuka M, Tierney K, Wallace WA, Von Winterfeldt D. A framework to quantitatively assess and enhance the seismic resilience of communities. Earthq Spectra 2003;19:733–52.

[20] An X, Yin Z, Tong Q, Fang Y, Yang M, Yang Q, Meng H. An integrated resilience assessment methodology for emergency response systems based on multi-stage STAMP and dynamic Bayesian networks. Reliab Eng Syst Safe 2023;238:109445. https://doi.org/10.1016/j.ress.2023.109445.

[21] Trucco P, Petrenj B. Characterisation of resilience metrics in full-scale applications to interdependent infrastructure systems. Reliab Eng Syst Safe 2023;235:109200. https://doi.org/10.1016/j.ress.2023.109200.

[22] Rose A. Economic resilience to natural and man-made disasters: multidisciplinary origins and contextual dimensions. Environ Hazards 2007;7:383–98. https://doi.org/10.1016/j.envhaz.2007.10.001.

[23] Zobel CW. Representing perceived tradeoffs in defining disaster resilience. Decis Support Syst 2011;50:394–403. https://doi.org/10.1016/j.dss.2010.10.001.

[24] Francis R, Bekera B. A metric and frameworks for resilience analysis of engineered and infrastructure systems. Reliab Eng Syst Safe 2014;121:90–103. https://doi.org/10.1016/j.ress.2013.07.004.

[25] Zobel CW, Khansa L. Characterizing multi-event disaster resilience. Comput Oper Res 2014;42:83–94. https://doi.org/10.1016/j.cor.2011.09.024.

[26] Zhang X, Mahadevan S, Sankararaman S, Goebel K. Resilience-based network design under uncertainty. Reliab Eng Syst Safe 2018;169:364–79. https://doi.org/10.1016/j.ress.2017.09.009.

[27] Zeng Z, Du S, Ding Y. Resilience analysis of multi-state systems with time-dependent behaviors. Appl Math Model 2021;90:889–911. https://doi.org/10.1016/j.apm.2020.08.066.

[28] Zeng Z, Fang Y, Zhai Q, Du S. A Markov reward process-based framework for resilience analysis of multistate energy systems under the threat of extreme events. Reliab Eng Syst Safe 2021;209:107443. https://doi.org/10.1016/j.ress.2021.107443.

[29] Yang Z, Xiang Q, He Y, Peng S, Faber MH, Zio E, Zuo L, Su H, Zhang J. Resilience of natural gas pipeline system: a review and outlook. Energies 2023;16:6237. https://doi.org/10.3390/en16176237.

[30] Tan Z, Wu B, Che A. Resilience modeling for multi-state systems based on Markov processes. Reliab Eng Syst Safe 2023;235:109207. https://doi.org/10.1016/j.ress.2023.109207.

[31] Dui H, Lu Y, Wu S. Competing risks-based resilience approach for multi-state systems under multiple shocks. Reliab Eng Syst Safe 2024;242:109773. https://doi.org/10.1016/j.ress.2023.109773.

[32] Liu J, Tian L, Yang M, Meng X. Probabilistic framework for seismic resilience assessment of transmission tower-line systems subjected to mainshock-aftershock sequences. Reliab Eng Syst Safe 2024;242:109755. https://doi.org/10.1016/j.ress.2023.109755.

[33] Koutras VP, Markov A. Regenerative process model for the dependability and performance of a two-unit multi-state system under maintenance. Reliab Eng Syst Safe 2023;238:109433. https://doi.org/10.1016/j.ress.2023.109433.

[34] Cheng D, Lu Z, Zhou J, Liang X. An optimizing maintenance policy for airborne redundant systems operating with faults by using Markov process and NSGA-II. Reliab Eng Syst Safe 2023;236:109257. https://doi.org/10.1016/j.ress.2023.109257.

[35] Bo Y, Bao M, Ding Y, Hu Y. A DNN-based reliability evaluation method for multi-state series-parallel systems considering semi-Markov process. Reliab Eng Syst Safe 2024;242:109604. https://doi.org/10.1016/j.ress.2023.109604.

[36] Song C, Xiao R, Zhang C, Zhao X, Sun B. Simulation-free reliability analysis with importance sampling-based adaptive training physics-informed neural networks: method and application to chloride penetration. Reliab Eng Syst Safe 2024;246:110083. https://doi.org/10.1016/j.ress.2024.110083.

[37] Wu B, Limnios N. A comparative study of numerical methods for reliability assessment based on semi-Markov processes. Reliab Eng Syst Safe 2024;252:110431. https://doi.org/10.1016/j.ress.2024.110431.

[38] Das S, Tesfamariam S. Reliability assessment of stochastic dynamical systems using physics informed neural network based PDEM. Reliab Eng Syst Safe 2024;243:109849. https://doi.org/10.1016/j.ress.2023.109849.

[39] Zhang C, Shafieezadeh A. Simulation-free reliability analysis with active learning and physics-informed neural network. Reliab Eng Syst Safe 2022;226:108716. https://doi.org/10.1016/j.ress.2022.108716.

[40] Zhou T, Zhang X, Droguett EL, Mosleh A. A generic physics-informed neural network-based framework for reliability assessment of multi-state systems. Reliab Eng Syst Safe 2023;229:108835. https://doi.org/10.1016/j.ress.2022.108835.

[41] Bo Y, Bao M, Ding Y, Hu Y. A DNN-based reliability evaluation method for multi-state series-parallel systems considering semi-Markov process. Reliab Eng Syst Safe 2024;242:109604. https://doi.org/10.1016/j.ress.2023.109604.

[42] Baydin AG, Pearlmutter BA, Radul AA, Siskind JM. Automatic differentiation in machine learning: a survey. J Mach Learn Res 2018;18:1–43.

[43] Yu T, Kumar S, Gupta A, Levine S, Hausman K, Finn C. Gradient surgery for multi-task learning. Adv Neural Inf Process Syst 2020;33:5824–36.

[44] Yang Z, Li X, Xiang Q, He Q, Faber MH, Zio E, Su H, Zhang J. A resilience evaluation method of natural gas pipeline system based on uncertainty analysis. Process Saf Environ 2023;177:891–908. https://doi.org/10.1016/j.psep.2023.07.058.

[45] Pei S, Zhai C, Hu J. Surrogate model-assisted seismic resilience assessment of the interdependent transportation and healthcare system considering a two-stage recovery strategy. Reliab Eng Syst Safe 2024;244:109941. https://doi.org/10.1016/j.ress.2024.109941.

[46] Wang N, Yuen KF. Resilience assessment of waterway transportation systems: combining system performance and recovery cost. Reliab Eng Syst Safe 2022;226:108673. https://doi.org/10.1016/j.ress.2022.108673.

[47] S. Ruder, An overview of gradient descent optimization algorithms, arXiv preprint arXiv:1609.04747, (2016).

[48] Xu Y, Kohtz S, Boakye J, Gardoni P, Wang P. Physics-informed machine learning for reliability and systems safety applications: state of the art and challenges. Reliab Eng Syst Safe 2023;230:108900. https://doi.org/10.1016/j.ress.2022.108900.

[49] Prechelt L. Automatic early stopping using cross validation: quantifying the criteria. Neural Netw 1998;11:761–7. https://doi.org/10.1016/S0893-6080(98)00010-0.

[50] Phaisangittisagul E. An analysis of the regularization between L2 and dropout in single hidden layer neural network. IEEE 2016:174–9. https://doi.org/10.1109/ISMS.2016.14.

[51] Srivastava N, Hinton G, Krizhevsky A, Sutskever I, Salakhutdinov R. Dropout: a simple way to prevent neural networks from overfitting. J Mach Learn Res 2014;15:1929–58.

[52] Pontes FJ, Amorim GF, Balestrassi PP, Paiva AP, Ferreira JR. Design of experiments and focused grid search for neural network parameter optimization. Neurocomputing 2016;186:22–34.

[53] Zhou T, Droguett EL, Mosleh A. Physics-informed deep learning: a promising technique for system reliability assessment. Appl Soft Comput 2022;126:109217. https://doi.org/10.1016/j.asoc.2022.109217.

[54] D.P. Kingma, J. Ba, Adam: A method for stochastic optimization, arXiv preprint arXiv:1412.6980, (2014). https://doi.org/10.48550/arXiv.1412.6980.